Enhanced Photocatalytic Degradation of Rose Bengal (RB) under Visible Light Irradiation by CTAB Modified Nickel Phosphate Nanocomposites

NIKHIL SANTHOSH[1], RENJUSHA SUDHARMONY AMMA[1], SUDHAKAR CHINNAVAR[2], ANAND SEKAR[3] and ARUNADEVI RAJA[4*]

[1]PG Department of Chemistry, N.S.S. College Pandalam- 689501, India

[2]Department of Chemistry, K.P. National College of Arts and Science, Batlagundu-624202, India

[3]Entamology Research Institute, Loyola College, Chennai-600034, India

[4]PG& Research Department of Chemistry, D.K.M. College for Women, Vellore- 632001, India

*Corresponding Author E-mail: arunarajan3@gmail.com

Abstract

The removal of Rose Bengal (RB) dye from aqueous solution using NiP/CTAB nanocomposites was studied. The NiP/CTAB nanocomposites were synthesized using simple co-precipitation method. The synthesized nanocomposites were charecterized by Spectral (UV-Vis DRS, FT-IR) and Analytical (PXRD, SEM, EDAX, HRTEM) techniques. Photodegradation of Rose Bengal dye using the synthesized catalyst was studied. NiP/CTAB nanocomposites exhibited excellent photocatalytic performance by degrading Rose Bengal (92%) at 0.2 g/L of catalyst and 10μM initial dye concentration at a pH of 8. The excellent performance by the catalyst is attributed to the highest electron hole pair generation. The kinetic study revealed that the photodegradation of Rose Bengal obeyed pseudo first order kinetics.

Keywords: NiP/CTAB nanocomposites, Rose Bengal Degradation, Photocatalyst,pseudo first order kinetics

Introduction

Water pollution is considered to be one of the biggest threat arose after the industrial revolution and the entire global population is facing its consequences. It’s adversely affecting the wild life, eco systems and of course the human society. One among the big hand in polluting our water resources is being contributed by the textile industry. Usage of textile dyes and their discharge to water bodies make the polluted and thereby affecting our

lives[1-2]. Rose Bengal (RB) or Acid Red 94 is a xanthene class of dye and commonly used in textile and printing industries, eye drops and it has also been used as an insecticide. These Xanthane dyes are reported to be genotoxic, cytotoxic and cytostatic[3-5]. The dissipation of RB causes severe health issues to the human beings. It targets the corneal epithelium of humans. It also causes skin itchiness, irritation and blistering of skin. It can lead to redness and inflammation of eyes. Also it can cause liver and stomach problems. These all aspects point that the degradation of Rose Bengal from water requires significant attention[6-7]. Conventional methods are there to degrade this dye such as adsorption, coagulation, sedimentation etc.[8,9]. However these methods have shortcomings such as incomplete degradation which is leading to secondary pollution, limited scope of use, low efficiency[10]. Semiconductor photocatalysis which falls in the category of Advanced Oxidation Process (AOP) has been proved to be a benign and enhanced method for the dye degradation. This environmental friendly technique works by the generation of reactive oxygen species like hydroxyl radicals with one unpaired electron which possess shorter life time. This follows by the rapid reaction of these species with various chemical species which are hard to degrade[11-13]. Cetyl trimethyl ammonium bromide (CTAB) is a cationic surfactant used in the production of nanocomposites and it controls the morphological structures, specific surface area and photocatalytic activity of the semiconductor photocatalyst[14,15]. Nickel phosphate (NiP) is an inorganic compound with the formula $Ni_3(PO_4)_2$. NiP is a semiconductor possesses strong absorption in the visible region[16]. In this work, we have synthesized NiP/CTAB nanocomposites by co-precipitation method. The synthesized nanocomposite is characterized by various spectroscopic, analytical and morphological techniques. Photocatalytic applications of the synthesized nanocomposite is evaluated by degrading Rose Bengal dye and the obtained results are compared with other photocatalysts and found that the synthesized catalyst exhibit excellent catalytic activity.

Experimental Section

Materials

Nickel Acetate ($C_4H_6NiO_4$), ortho phosphoric Acid (H_3PO_4), Cetyl trimethylammonium bromide (CTAB) and sodium hydroxide (NaOH) were purchased from MERCK. The chemicals were of analytical grade and used without further purification. Double distilled water was used throughout the experiment.

Synthesis of Nickel phosphate (NiP) nanoparticles

The nickel phosphate was synthesized by following the simple co-precipitation method. Initially 5g of $C_4H_6NiO_4$ was dissolved in 50 ml double distilled water. 3 ml of H_3PO_4 solution was added carefully to this solution to form the mixture. A further addition of freshly prepared NaOH was done drop by drop into the above mixture under vigorous stirring. Followed by the addition, the whole mixture was stirred at room temperature for 3 h lead to the formation of precipitate. It was further filtered, washed with ethanol and dried at 100 ^{0} C for 2 h. Finally the obtained precursor was calcinated in muffle furnace at 200 ^{0} C for 2 h.

Synthesis of NiP /CTAB nanocomposites

NiP/ CTAB nanocomposite was synthesised by following the sonochemical method. 3 g of Nickel phosphate and 1 g of CTAB were dissolved in 40 ml ethanol trailed by sonication for 30 minutes. The mixture was then subjected to vigorous stirring at room temperature for 3h. The precipitate attained was filtered, washed with ethanol and dried at 100^{o}C to finally obtain the nanocomposite.

Materials Characterization

The UV- Vis diffuse reflectance spectral measurements for dry-pressed disk samples were carried out in a JASCOV-550 double beam spectrophotometer with PMT detector equipped with an integrating sphere assembly, using $BaSO_4$ as a reference sample. The spectrum was recorded at room temperature in the wavelength range from 200 nm to 800 nm. Functional group analysis of synthesized samples were carried out by Shimaszu Fourier Transform Infrared Spectrometer (IR Affinity-1) using KBr- nanocomposite mixture in the form of pellets. The structure and phase details of the samples were determined by X-ray powder diffraction with Cu Kα radation at 25^0 C using XPERT PRO. The surface morphology was analysed by Scanning Electron Microscopy using JM 6701F-6701 instrument in both secondary and backscattered electron modes. The elemental analysis was conducted by an energy dispersive X-ray spectroscopy (EDX) attached to the (SEM).

Photocatalytic measurements

The photocatalytic activities of the as synthesized samples were evaluated by the degradation of rose bengal under visible light irradiation. The photocatalytic experiments were conducted in a jacketed cylindrical quarts photoreactor. Visible light was obtained using a 300 xenon arc lamp with a 420 nm cutoff filter to ensure the irradiation light was perfect. The reaction temperature was maintained at 25 ^{0} C by circulating water in the cooling jacket of the photoreactor. 0.15 g NiP /CTAB was dispersed in a 300 ml rose bengal solution. Prior to visible light irradiation, the rose bengal solution containing the photocatalyst was magnetically stirred for 30 minutes in the dark to ensure the adsorption band at 544 nm in the UV visible spectra of rose bengal using a JASCO UV- vis spectrometer 530. The percentage of photodegradations of rose bengal was calculated by the following formula.

$$\textbf{Photodegradation (\%)} = C_0\text{-}C/C_0 \text{ X } 100$$

Where,

$\mathbf{C_0}$ is the concentration of phenol before irradiation time.

C is the concentration of phenol after a certain irradiation time

Results and Discussion

PXRD Analysis

XRD patterns of NiP and NiP /CTAB nanocomposites were recorded to understand the crystal nature of the synthesized nanocomposite. Figure 1 displays the XRD patterns. The analysis confirmed that NiP and NiP /CTAB were crystalline in nature. The sharp peak at 11.6° correspond to the (020) crystal planes of NiP according to standard card no.33-0951[17]. No peaks of other phosphites or phosphates were detected from these patterns. The peaks are sharp and strong, which indicates the good crystallinity of the as-prepared samples. Also no diffraction peaks regarding the CTAB was found which may suggest the amorphous phase of CTAB. Good crystallinity NiP /CTAB might improve the cycle life of the photocatalyst for its relatively stable structure in the photochemical process. The average crystalline size of NiP and NiP /CTAB was examined by Full Width Half Maximum value of prominent diffraction peak of the XRD pattern using Scherer's equation as follows.

$$\mathbf{D = K\lambda / \beta\cos\theta}$$

where β is the Full Width Half Maximum (FWHM) of the 2θ peak, K is the shape of factor of the particles (it equals to 0.9), θ and λ are the incident of angle and the wavelength of the X-rays respectively The average crystalline size of NiP and NiP /CTAB was found to be 21.50 nm and 6.09 nm respectively.

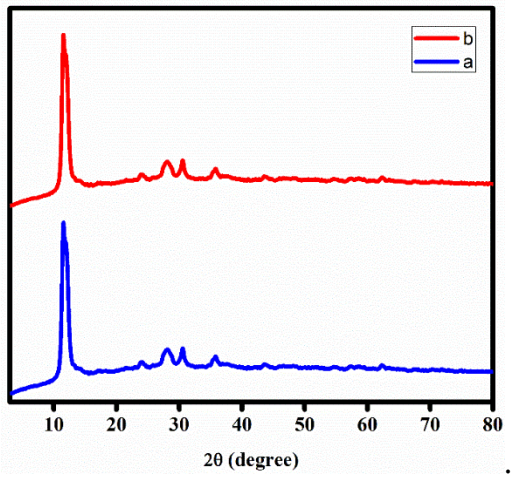

Fig 1. XRD patterns of (a) NiP (b) NiP /CTAB nanocomposites

FT-IR Analysis

The FT-IR spectra of pure NiP and the NiP /CTAB nanocomposites are shown in Fig 2. In Fig. 2 (a) the peak near to 1000 cm^{-1} may be attributed to the asymmetric stretching vibration of (PO_4^{3-}) [16]. The FT-IR spectrum of NiP /CTAB nanocomposites (Fig 2 (b)) shows a band at 758.02cm^{-1} that could be assigned to the vibrations of the ammonium moiety in CTAB. Peaks at 904.61 and 1629.85 cm^{-1} are attributed to two different CH bands vibration of the CH_2 group in CTAB. The bands at 3576.02 and 758.02 cm^{-1} belong to asymmetric and symmetric stretching vibration of N^+- CH_3, while the band at 1629.85 cm^{-1} corresponds to the out-of-plane-CH vibration of CH_3. The band at 904.61 cm^{-1} could be assigned to Br^-. The FTIR spectrum of NiP /CTAB nanocomposite displays a peak at 3377.36 cm^{-1} which is a CTAB band and it proves the composite formation[18]. The broadband at 2069.62 cm^{-1} might be assigned to the electrostatic interaction between hydroxyl groups at NiP surface and the ammonium moiety in CTAB.

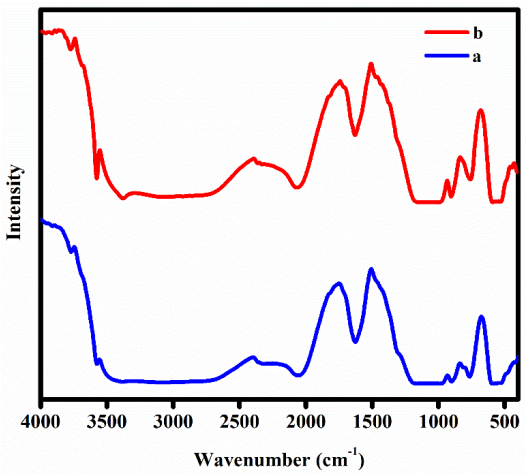

Fig 2. FT-IR spectra of (a) NiP (b) NiP /CTAB nanocomposites

UV-Vis-DRS Analysis

The UV-vis diffuse reflectance spectra (UV-Vis-DRS) of pure NiP together with the NiP /CTAB nanocomposites are shown in Fig 3 (A). It could be observed that bare NiP exhibited a strong absorption band in the range of 350-500 nm and from 600 to 800 nm , associated with the intrinsic band gap absorption of (Ni^{2+})[16] whereas pure NiP /CTAB nanocomposites had a strong and broad absorption with absorption edge at about 530 nm. Compared to pure NiP, as expected, the hierarchical NiP /CTAB nanocomposites depicted enhanced visible light absorption, especially in the range of 530 nm. It was noted that the colour of the samples changed from yellow to grey when more and more black CTAB were introduced into the pure NiP nanoparticles. This interesting and prominent enhancement of the visible light absorption of the hierarchical NiP /CTAB nanocomposites could be ascribed to the interaction between NiP and CTAB, which could significantly improve the light harvesting effcienty of NiP in the visible light region, and then produce more photogenerated charge carries to participates in the photocatalytic degradation process, leading to superior photocatalytic efficiency under visible light irradiation. The band gap energies of NiP and CTAB were calculated by the following formula,

$$(\alpha h\nu)^{1/\gamma} = B(h\nu - E_g)$$

Where h- Planck constant, α- absorption coefficient, *v*- photon's frequency, E_g- Band gap energy and B- Proportionality constant, respectively. The value of γ depends on the transition and is ½ for direct and 2 for indirect transition band gaps[19]. The E_g values were estimated by extrapolation of the linear part of the curves obtained by plotting $(\alpha h\nu)^2$ versus *hv* as shown in Fig. 3 (B&C). The values of Eg for NiP and NiP /CTAB nanocomposites

were estimated to be 5.0 eV and 1.41 eV, respectively. This shows NiP /CTAB nanocomposites should possess excellent visible light driven photocatalytic activity due to its narrow band gap.

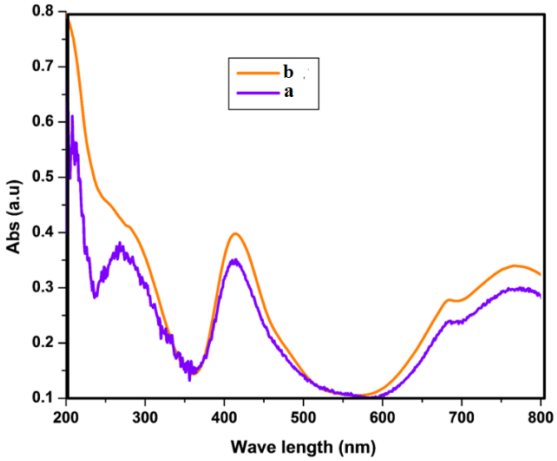

Fig.3. (A) UV-vis-DRS spectra of (a) NiP (b) NiP /CTAB nanocomposites

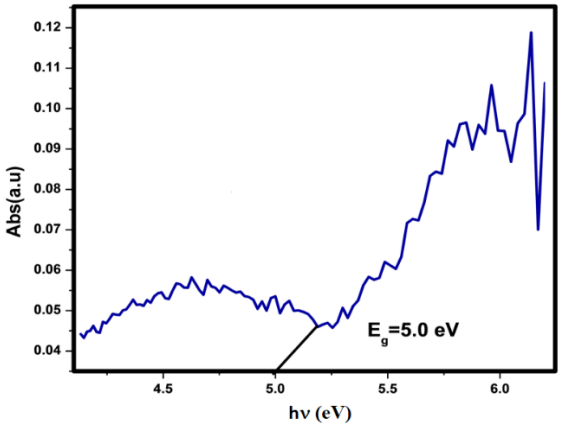

Fig.3 (B). Tauc plots of NiP

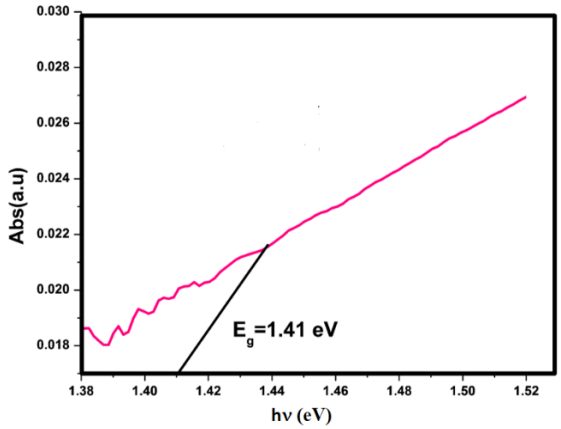

Fig.3 (C) Tauc plots of NiP /CTAB nanocomposites

SEM & EDX Analysis

Morphology of the as-prepared samples was investigated using SEM analysis and the results are shown in Fig. 4. This structure was conducive to the entrance of visible light and rapid transfer of photo-generated charge carriers, further enhancing the catalytic activity of the material. NiP shows needles like structures and NiP /CTAB nanocomposites exhibits needle with flakes structures.

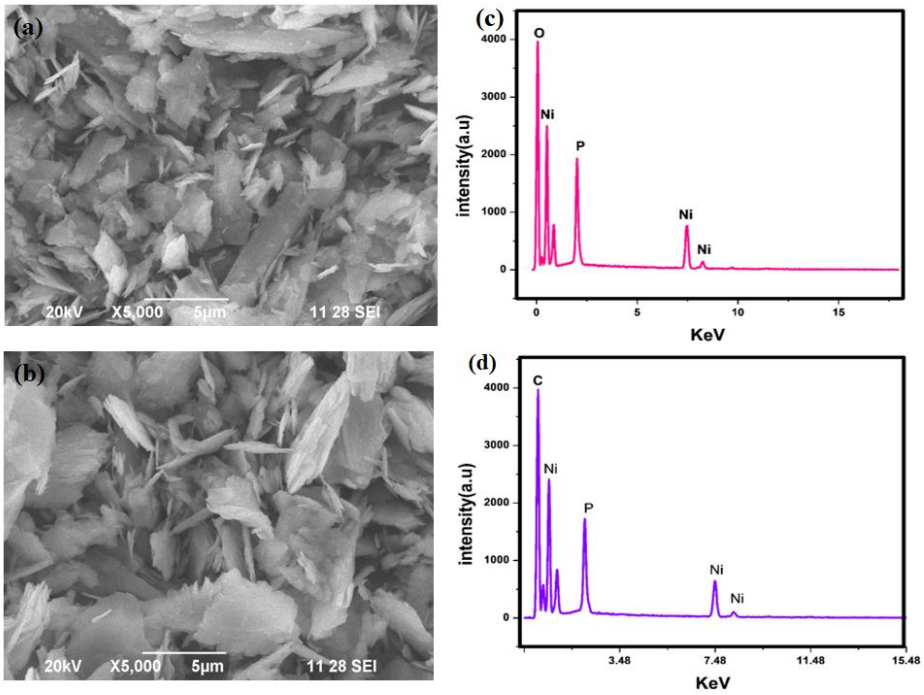

Fig 4. SEM images of (a) NiP (b) NiP /CTAB nanocomposites
(c) EDX image of NiP (d) EDX image of NiP /CTAB nanocomposites

The EDX spectra also recorded to confirm purity of the NiP/CTAB nanocomposites and the result are given in Fig. 4 (d) It can be seen clearly that the existence of Ni and P elements in the NiP and Ni, P and C elements in the NiP /CTAB nanocomposites

Photocatalytic Activity

Photodegradation of Rose Bengal

The photocataytic activity of the synthesized nanocomposites was evaluated by performing the degradation of Rose Bengal under visible light irradiation. The photodegradation was studied by checking the characteristic absorption band of Rose Bengal (λ_{max} = 545 nm) as shown in Fig.5 (a). The absorption intensity was found to be decreasing significantly with increase in reaction time indicating the degradation of Rose Bengal. Fig.5 (b) displays the photocatalytic performances of pure NiP, NiP /CTAB nanocomposites and in the absence

of photocatalyst for same initial concentration of Rose Bengal. As can be seen, that in absence of any photocatalyst, the concentration of Rose Bengal remains unchanged indicating the stability of Rose Bengal under visible light. Prior to the irradiation, the adsorption of Rose Bengal was checked for 30 min for all catalysts and found to be negligible. The NiP /CTAB nanocomposites showed enhanced photodegradation of Rose Bengal compared to pure NiP under visible light irradiation[20].

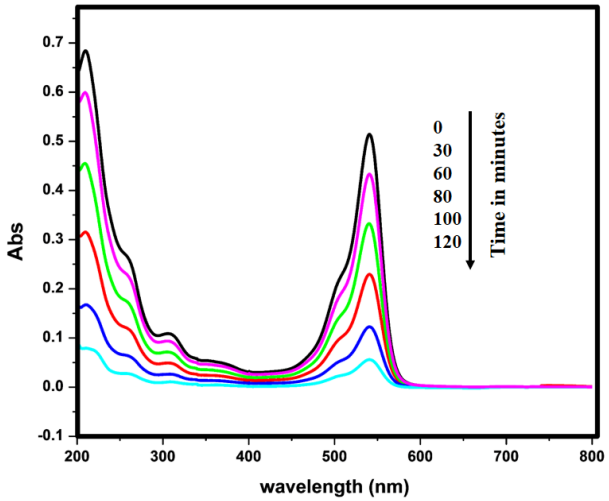

Fig 5 (a) Time dependent UV-vis spectral changes of RB in the presence of NiP and NiP /CTAB nanocomposites under visible light irradiations

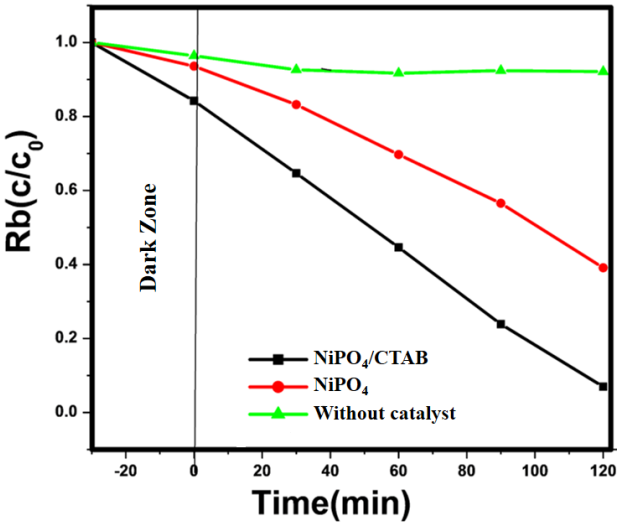

Fig 5 (b) Photodegradation curve of RB using NiP and NiP /CTAB nanocomposites

Kinetics of Photodegradation of Rose Bengal

The kinetics of photocatalytic degradation of rose Bengal was also investigated. The degradation of Rose Bengal was found to be following the pseudo-first-order kinetics (Plots of -ln (C/C_0) vs time showed linear relationship).

$$\mathbf{- \ln (C/C_0) = kt}$$

Where C is the concentration of Tartrazine remaining in the solution at irradiation time t and C_0 is the initial concentration at t = 0. First order rate constant was evaluated from the slope of the -ln (C/C_0) vs time plots shown in Fig. 6.

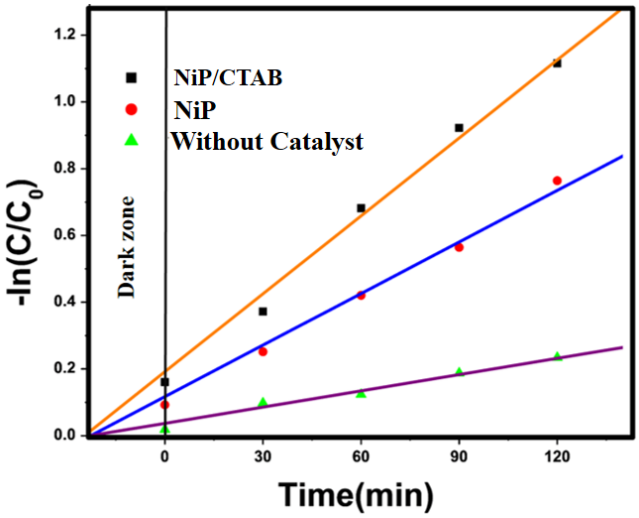

Fig 6. Kinetic regime on the photodegradation of RB in the presence of NiP /CTAB nanocomposites

Mechanism of Rose Bengal degradation by NiP /CTAB nanocomposites

The degradation of Rose Bengal by NiP /CTAB nanocomposites can be explained as follows. The schematic diagram of electron transfer in NiP /CTAB under visible light irradiation is shown in Fig. 7. It can be explained as follows; when NiP /CTAB is irradiated by visible light, photogenerated electrons moves from the valance band to the conduction band and leave holes in valance band. This leads to the generation of electron – hole pair. The absorbed oxygen molecules at the surface of the catalyst react with the excited electron and produce the superoxide radical anion $O_2^{\bullet}$. This superoxide radical anions get protonated and forms HOO^-. Similarly the holes (h^+) remained in the valance band reacts with H_2O to generate OH^- radicals. Finally these reactive species interact with the dye molecules and degrade them into CO_2 and H_2O[21].

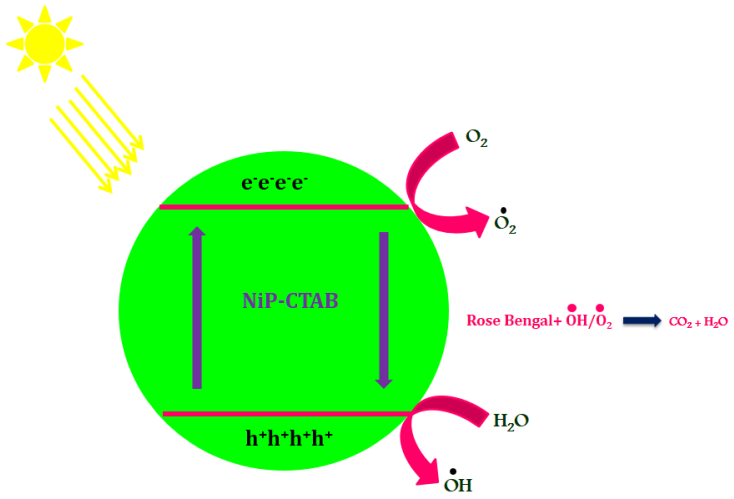

Fig 7. Mechanism of RB degradation by NiP /CTAB nanocomposites

Effect of NiP /CTAB dosage

The effect of catalyst on the photodegradation of Rose Bengal was analyzed by varying the concentration of NiP /CTAB from 0.05 g/L to 0.3 g/L for 10 μM Rose Bengal and the results are shown in Fig. 8. It exhibited the superior rate of degradation at the NiP /CTAB concentration of 0.2 g/L. The rate of degradation was found to be increased with the increasing concentration of nanocomposites from 0.05 g/L to 0.2 g/L. And the highest degradation (92%) occurred at 0.2 g/L. This is due to the surge in the availability of active sites at the surface of the catalyst. But a further increase in the catalyst concentration resulted in a decrease in the degradation rate. This may be attributed to the shielding of the penetrating light by the excessive amount of catalyst[20].

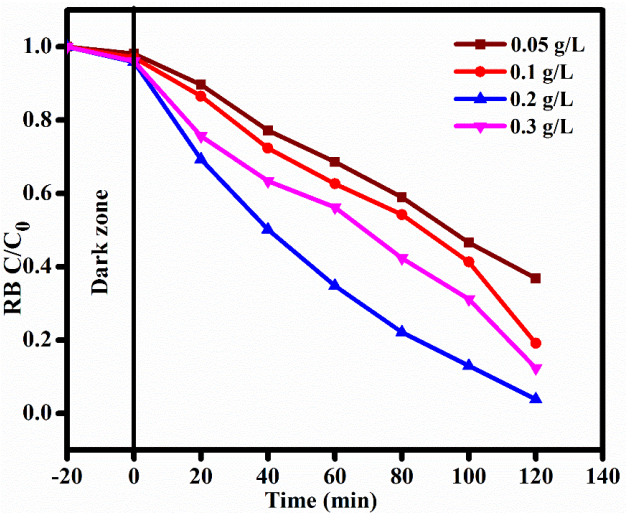

Fig 8. Effect of NiP /CTAB dosage on the photodegradation of RB

Effect of initial Rose Bengal concentration

The effect of initial concentration of Rose Bengal on rate of photodegradation is illustrated in Fig. 9. The influence of initial concentration of Rose Bengal on rate of degradation was studied by increasing the concentration from 5 to 15µM at a fixed concentration of catalyst at 0.2g/L. Photocatalytic degradation increases with increase in the concentration of dye up to 10µM and record the highest degradation (92%). This may be attributed to the fact that as the concentration of the dye increased, more dye molecules will be available for excitation and energy transfer which increases the percentage of degradation. But beyond 10µM of the dye concentration, the degradation is showing a decrease. This may be due to the fact that at higher concentration dyes start covering the surface of photocatalyst and therefore reducing the light intensity.

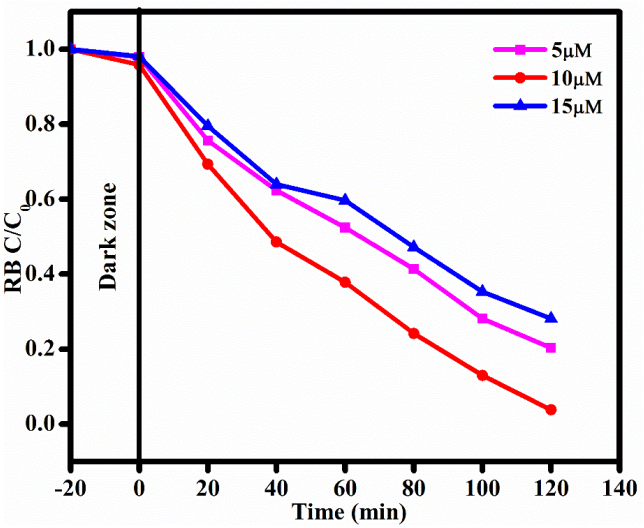

Fig 9. Effect of RB concentration on the photodegradation

Effect of pH

The effect of pH of the solution on the photodegradation of Rose Bengal was studied by performing the reaction under various pH ranging from 3 to 9 for dye concentration 10 µM and Catalyst dosage 0.2 g/L and the results are shown in Fig.10. It was found that as we increased the pH, better photodegradation was happening and highest degradation (92%) was at pH= 8. As the pH increased from 3 to 9, the degradation percentage increased initially but after pH 8, it decreased. Under the lower pH value, the anionic dye in their protonated form and catalyst also owns positive charge due to adsorption of H^+ ions. So, in the acidic medium, the dye molecule repel from the catalyst and shows lower degradation rate[22]. The better degradation as we increase the pH may be due to generation

of more •OH radicals, which are produced from the interaction of OH− and hole (h+) of the semiconductor. These •OH radicals are responsible for the oxidative degradation of dye. The rate decreases after certain pH because more OH^- ions are available at higher pH and these will be adsorbed on the surface of the semiconductor making it negatively charged so that the approach of anionic form of Rose Bengal towards semiconductor surface will be retarded due to repulsion[23].

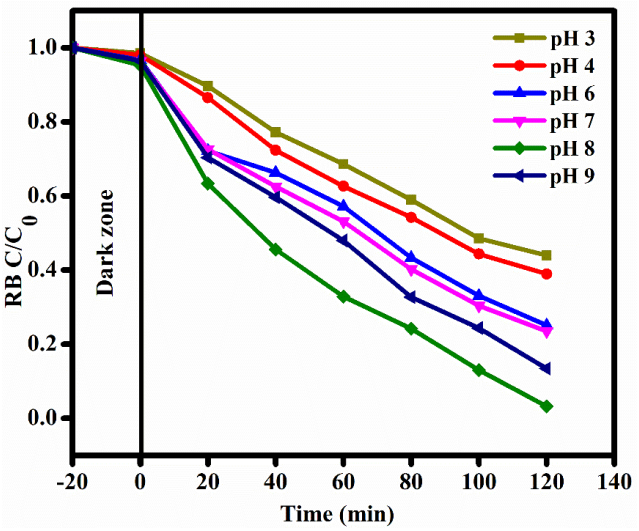

Fig 10. Effect of pH on RB degradation

Conclusion

The NiP /CTAB nanocomposite was successfully synthesized by co-precipitation method as an efficient photocatalyst for the removal of Rose Bengal dye from aqueous solution. The as synthesized nanocomposite was characterized by various spectroscopic, analytical and morphological techniques. The (NiP /CTAB nanocomposite was studied for the photodegradation of Rose Bengal dye in aqueous solution and displayed excellent results under the visible light irradiation compared with pure NiP nanoparticles. The optimum catalyst loading for the highest degradation (92%) was observed as 0.2 g/L and the optimum initial concentration of dye as 10µm in aqueous solution. The optimum pH for the photodegradation to happen was found to be pH 8. The kinetic study revealed that the photodegradation of Tartrazine obeyed pseudo first order kinetics. The catalyst was found successful in degrading the dye into organic components water (H_2O) and Carbon dioxide (CO_2).

Acknowledgements

The Authors thank School of Chemistry, Madurai Kamaraj University for providing laboratory facilities to carry out this work. The authors thank the management of C.P.A. College, Tamilnadu, DST FIST Lab, D.K.M. College for Women (Autonomus), Vellore, Tamilnadu, DST FIST Sponsored Post Graduate Department of Chemistry, N.S.S. College, Pandalam, Kerala for providing instrumental facilities for this work.

Conflicts of Interest

The authors declare that there is no conflicts of interests regarding the publication of this article.

References

1. S. Ameen, Hyung-Kee Seo, M. Shaheer Akhtar, and Hyung Shik Shin. *Chemical engineering journal* **210**, 220-228 (2012) https://doi.org/10.1016/j.cej.2012.08.035
2. S. Shweta, Rakshit Ameta, R. K. Malkani, and S.C. Ameta. *Journal of the Serbian Chemical Society*, **78**, 897-905 (2013) http://dx.doi.org/10.2298/JSC120716141S
3. Fara Maria Drumond Chequer, Vinícius de Paula Venâncio, Maria de Lourdes Pires Bianchi, and Lusânia Maria Greggi Antunes. *Food and Chemical Toxicology*, **50**, 3447-3451 (2012) https://doi.org/10.1016/j.fct.2012.07.042
4. S. Ameen, Doo-Ri Park, and Hyung Shik Shin. *Journal of Materials Science: Materials in Electronics*, **27**, 10460-10467 (2016) https://doi.org/10.1007/s10854-016-5135-8
5. Sako, Fumiyo, Noriko Kobayashi, Hiroyuki Watabe, and Naoyuki Taniguchi, *Toxicology and applied pharmacology*, **54**, 285-292 (1980) https://doi.org/10.1016/0041-008X(80)90198-2
6. B. Malini, and G. Allen Gnana Raj, *Journal of environmental chemical engineering*, **6**, 5763-5770 (2018) https://doi.org/10.1016/j.jece.2018.09.002
7. K. Vignesh, R. Hariharan, M. Rajarajan, and A. Suganthi, *Solid state sciences*, **21**, 91-99 (2013) https://doi.org/10.1016/j.solidstatesciences.2013.04.017
8. B. H. Hameed, A.T.M. Din, and A. L. Ahmad. *Journal of hazardous materials* 141, 819-825 (2007) https://doi.org/10.1016/j.jhazmat.2006.07.049
9. Marco Derudi, Gianluca Venturini, Giorgio Lombardi, Giuseppe Nano, and Renato Rota, *European Journal of Soil Biology*, **43**, 297-303 (2007) https://doi.org/10.1016/j.ejsobi.2007.03.001

10. M. A. Rauf, N. Marzouki and Bahadir K. Körbahti, *Journal of Hazardous Materials*, **159**, 602-609 (2008) https://doi.org/10.1016/j.jhazmat.2008.02.098
11. R. Satheesh, K. Vignesh, Ahmed Abdel-Wahab, A. Suganthi, and M. Rajarajan, *The Canadian Journal of Chemical Engineering*, **96**, 1713-1722 (2018) https://doi.org/10.1002/cjce.23122
12. V. Ramasamy Raja, D. Rani Rosaline, A. Suganthi, and M. Rajarajan, *Ultrasonics sonochemistry*, **44**, 73-85 (2018). https://doi.org/10.1016/j.ultsonch.2018.02.043
13. S. Selvarajan, A. Suganthi, M. Rajarajan, and M. M. Shrividhya, *Optik-International Journal for Light and Electron Optics*, **153**, 16-30 (2018) https://doi.org/10.1016/j.ijleo.2017.09.082
14. Narenuch, Teerapong, Teeradech Senasu, Tammanoon Chankhanittha, and Suwat Nanan, *Journal of Solid State Chemistry*, **294**, 121824 (2021) https://doi.org/10.1016/j.jssc.2020.121824
15. Soheila Abdi and Davoud Dorranian, *Optics & Laser Technology*, **108**, 372-377(2018) https://doi.org/10.1016/j.optlastec.2018.07.009
16. Wang Yaning, Wang Kang and Wang Xitao, *Journal of colloid and interface science*, **466**, 178-185 (2016) https://doi.org/10.1016/j.jcis.2015.12.021
17. Tianyu Zhan, Haoyong Yin, Jiajie Zhu, Junli Chen, Jianying Gong, Ling Wang, and Qiulin Nie, *Journal of Alloys and Compounds*, **786**, 18-26, (2019) https://doi.org/10.1016/j.jallcom.2019.01.304
18. Japinder Kaur and Sonal Singhal, *Physica B: Condensed Matter*, **450**, 49-53 (2014) https://doi.org/10.1016/j.physb.2014.05.069
19. Patrycja Makuła, Michał Pacia, and Wojciech Macyk, J. Phys. Chem. Lett., **9,** 6814-6817(2018) https://pubs.acs.org/doi/abs/10.1021/acs.jpclett.8b02892
20. Priti Bansal and Dhiraj Sud, *Desalination*, **267**, 244-249 (2011) https://doi.org/10.1016/j.desal.2010.09.034
21. K. Bhuvaneswari, T. Pazhanivel, G. Palanisamy, and G. Bharathi, *Journal of Materials Science: Materials in Electronics*, **31,** 6618-6628 (2020). https://doi.org/10.1007/s10854-020-03217-w
22. G.Murugadoss, D. Dinesh Kumar, M.Rajesh Kumar, N. Venkatesh, P. Sakthivel, *Sci Rep*, **11**, 1080 (2021) https://doi.org/10.1038/s41598-020-79993-6
23. Khushnuma Parveen and Ritu Vyas, *Acta Chim. Pharm. Indica*, **6**, 135-143 (2016)